

Physics of accretion onto young stars

III. Comparisons with observations

L. Siess, M. Forestini, and C. Bertout

Observatoire de Grenoble, Laboratoire d'Astrophysique, Université Joseph Fourier, B.P. 53X, F-38041 Grenoble Cedex, France

Received 14 April 1998 / Accepted 12 November 1998

Abstract. We present new evolutionary sequences for long lasting accreting low-mass ($0.1 M_{\odot} \leq M \leq 2.5 M_{\odot}$) pre-main sequence stars. The calculations, performed for two different mass accretion rates, show that accretion accelerates the evolution of the star. The star has a smaller radius and goes down its convective track faster than in a standard scheme. Consequently, the age of a star, as given by its location on the Hertzsprung-Russell diagram, is lower than that of a non-accreting star. We discuss ^2H and ^7Li burning and show how accretion affects the surface abundance of these elements. Notably, we point out that deuterium must be present at the surface of accreting intermediate-mass stars. Finally, we estimate the age, mass and radius of a sample of T Tauri stars located in the Taurus Auriga star forming region.

Key words: accretion, accretion disks – stars: abundances – stars: evolution – stars: fundamental parameters – stars: pre-main sequence

1. Introduction

The gravitational collapse of an initially rotating molecular cloud core model was recently computed by several groups (e.g. Yorke et al. 1993, 1995), who solved numerically the hydrodynamical equations governing the collapse. These computations show the formation of a central protostar surrounded by a flattened, disk-like structure in the equatorial plane of the initial cloud. Addition of an initial uniform magnetic field threading the cloud core does not change this result (Galli & Shu 1993). After being predicted by theoretical computations, the presence of disks around young stellar objects (YSOs) is now confirmed by HST observations (Burrows et al. 1996). There are many reasons to believe that circumstellar disks around young stars are in fact accretion disks as defined by Lynden-Bell & Pringle (1974), notably the outflow activity observed during the early phases of stellar evolution (Shu et al. 1994ab, Ferreira & Pelletier 1995).

An accretion disk is characterized by two parameters, the accretion rate \dot{M}_{acc} and the disk survival time t_{disk} . The first quantity can be inferred from the relation

$$\dot{M}_{acc} = \frac{2RL_{disk}}{GM},$$

where L_{disk} is the disk luminosity (determined from a disk model), R and M the stellar radius and mass, respectively. Adopting a mean stellar mass equal $0.5 M_{\odot}$ and mean radius of $2R_{\odot}$, Adams et al. (1990) derived accretion rates in the range $4 \cdot 10^{-8} < \dot{M}_{acc} < 4 \cdot 10^{-6} M_{\odot} \text{ yr}^{-1}$. Independent derivations provided by the observation of optical and near-UV excess emission lead to similar values (Bertout & Basri 1989, Hartmann & Kenyon 1990, Hartigan et al. 1995). Using the main-sequence mass-luminosity relation to derive the stellar mass and the effective temperature-spectral type relation of Cohen & Kuhi (1979), Hillenbrand et al. (1992, hereafter HSVK) found accretion rates in the range $6 \cdot 10^{-7} < \dot{M}_{acc} < 8 \cdot 10^{-5} M_{\odot} \text{ yr}^{-1}$, for intermediate-mass stars. Note however that derivations of accretion rates suffer from large uncertainties. Direct estimates of the intrinsic disk luminosity are difficult, and the exact geometry of mass accretion onto young stars is still a matter of debate (cf. Bertout et al. 1996).

The other major disk parameter, the disk lifetime, is roughly given by $t_{disk} \sim M_{disk}/\dot{M}_{acc}$, where M_{disk} is the disk mass. This value represents however a lower limit because of the possible replenishment of the disk by material from surrounding envelope. Evaluation of disk masses depends crucially on the opacity in the submillimeter and millimeter ranges, which are still relatively poorly known. For intermediate-mass stars, one finds that t_{disk} is of order of 0.3 Myr (HSVK). This time-scale is comparable to the age of the central star and suggests that the disk should be replenished by ambient circumstellar material, cold and transparent enough to have escaped detection in the millimeter range. Such a large reservoir of material surrounding the star-disk system is also invoked if a relatively high mass loss rate ($\dot{M}_{wind} \sim 10^{-7} M_{\odot} \text{ yr}^{-1}$; Edwards et al. 1993) is maintained for several Myr.

Observations of low-mass T Tauri stars (e.g. Walter et al. 1988, Strom et al. 1989, Neuhäuser et al. 1995a) indicates that disk survival times are different from star to star and span a large range between $10^6 - 10^7$ yr. This wide distribution of disk survival times is also required to explain the rotational evolution of low-mass stars (e.g. Bouvier et al. 1997a, Krishnamurthi et al. 1997). The presence of a binary companion is another factor that may influence disk lifetimes and the geometry of accretion.

A close companion is supposed to clean the central parts of the primary circumstellar disk and lead to a circumbinary disk. However, recent observations (Bouvier et al. 1997b) seems to indicate that the presence of a companion does not prevent accretion from occurring onto the primary at a rate similar to that observed in single PMS stars.

If the star is accreting continuously during a period t_{disk} , then the mass of the circumstellar matter should be in the range

$$0.1M_{\odot} \lesssim [t_{disk} \times \dot{M}_{acc}] \lesssim 1M_{\odot},$$

values consistent with other determinations (Adams et al. 1990, Beckwith et al. 1990, HSVK). Hence, a substantial amount of matter must transit through the disk and feed the star. The fraction of accreted material expelled by jets or outflows surrounding YSO probably does not exceed a few percent (Hartigan et al. 1995). Consequently a large amount of matter is deposited onto the star and must alter the pre-main sequence evolutionary paths followed by accreting stars. The evidence gathered to date suggests that the fraction of PMS stars which display IR excesses compatible with the presence of accretion disks lies between a few percents, when including X-ray discovered young stars in large areas (e.g. Alcalá et al. 1996, Neuhäuser et al. 1995b, Wichmann et al. 1996) and $\sim 50\%$, when considering only small cloud core regions (e.g. Beckwith and Sargent 1993). Observations also indicate that the frequency of optically thick disks evolves with time; between 60–100% of the youngest stars in the central parts of molecular cloud are surrounded by circumstellar material and by an age of ~ 10 Myr only 10–30% of these T Tauri stars still exhibit disks features (e.g. Strom 1995). These stars are surrounded initially by massive, optically thick accretion disks, evolving on time scales $t < 10$ Myr for solar-type stars and $t < 1$ Myr for intermediate-mass stars (Strom & Edwards 1993).

As noted previously, the ROSAT detection of X-ray emitting PMS without IR excesses in large areas around star forming regions have considerably reduce the frequency of disks among TTS to a few percents (e.g. Neuhäuser et al. 1995b). However, datation of these sources, by comparison with theoretical PMS evolutionary tracks (e.g. Alcalá et al. 1997, Wichmann et al. 1997), indicates that a large fraction of these objects are indeed weak line T Tauri stars, in a later evolutionary status, with ages larger than 10 Myr. These observations thus confirm the decreasing disk frequency with age, and also indicate that the dissipation of the disk is probably short, of the order of $\sim 10^5$ yr (Wolk & Walter 1996).

Accretion rates of $10^{-7}M_{\odot} \text{ yr}^{-1}$ and disk lifetimes of $\sim 5 \cdot 10^6$ yr seem to be reasonable values. These numbers lead to a total amount of accreted matter of the order of $\sim 0.5 M_{\odot}$. Although the accreted mass is much larger than the solar system mass, planetary system might be formed in the inner part of the disks. From a theoretical point of view, two typical models have been proposed so far for the formation of solar system; the models with a low mass nebula of $\sim 0.02 M_{\odot}$ (Hayashi et al. 1985, Safranov & Ruzmaikina 1985) and the models developed by Cameron and his co-workers, with high mass nebula of $\sim 1 M_{\odot}$ (Cameron & Pine 1973, DeCampli & Cameron 1979, Cameron

1985). Our models would then be included in the high mass nebula models, but one has to keep in mind that disk replenishment is invoked and that $0.5 M_{\odot}$ represents the total accreted mass and not the effective mass of the circumstellar disk.

In the next section, we briefly describe the evolutionary code and the accretion model. In Sect. 3, we study the structure and evolution of stars accreting at two different rates. In Sect. 4 we compare our models with standard ones (i.e. without accretion) and we focus on the consequences of accretion on the mass and age determinations. In Sect. 5, we discuss the observational effects of accretion on the surface ^2H and ^7Li abundances. In Sect. 6 we use our new grids of models to estimate the age and mass of a sample of T Tauri stars from the Taurus-Auriga star forming region. Sect. 7 contains a discussion and comparisons with other works and the paper concludes with a summary in Sect. 8.

2. Input physics

2.1. The accretion model

The stellar evolution code used in these computations is described by Forestini (1994). The accretion model was developed by Siess & Forestini (1996, hereafter Paper I) and treats the accretion process in one dimension. The mass deposition profile inside the star is derived as a function of the chemical and thermal properties of the accreted matter. The model also takes into account its angular momentum. Simulations have shown that the accreted material penetrates below the thin radiative envelope of low-mass stars and rapidly reaches the center of these completely convective stars. It has also been demonstrated that a radiatively stable layer acts as a barrier and stops matter penetration.

The structure and evolution of accreting stars has been described in detail by Siess et al. (1997a, hereafter Paper II). Their work shows that accretion leads to energetic changes that are able to significantly influence the global stellar evolution. In particular, this paper discusses the role of deuterium burning during accretion. The rapid reaction rate of $^2\text{H}(p,\gamma)^3\text{He}$ (typically a few hundred years or less) and its key role for the stellar energetics make it necessary to couple the deuterium nucleosynthesis process to the stellar structure equations. The equation governing the deuterium abundance evolution is

$$\frac{dn}{dt} = -\frac{n}{\tau_{dest}} + \frac{n}{\tau_{prod}} + \frac{n_D^a}{\Delta t}, \quad (1)$$

where τ_{dest} and τ_{prod} represent the characteristic time scales of, respectively, deuterium burning and deuterium production in the nuclear reactions $^2\text{H}(p,\gamma)^3\text{He}$, $2p(\gamma,\nu)^2\text{H}$ and $^9\text{Be}(p,^2\text{H})2^4\text{He}$. n is the deuterium number density and n_D^a the deuterium number density accreted over the current time step Δt , in a given shell.

In addition to nuclear energy release, the accreted matter also locally deposits a fraction α of the available accretion energy L_{bl} released in the boundary layer, so that the equation of energy conservation writes

$$\frac{\partial L_r}{\partial m} = \varepsilon_{nuc} + \varepsilon_{grav} + \varepsilon_{acc}, \quad (2)$$

where L_r is the local luminosity, ε_{acc} the specific accretion energy released per second (its expression is given in paper II) and ε_{nuc} (ε_{grav}) the nuclear (gravitational) energy production rate per unit mass, respectively. Integration of Eq. (2) over the interval $[0, M]$ leads to

$$L = L_{nuc} + L_{grav} + \alpha L_{bl}, \quad (3)$$

where L is the emergent stellar luminosity, L_{nuc} and L_{grav} the nuclear and gravitational ones, respectively. αL_{bl} represent the fraction of the accretion energy deposited in the boundary layer which is given to the star ($L_{bl} = \mathcal{G}M\dot{M}_{acc}/2R$). Finally, to account for the mass deposition, the new mass shell dm at time $t + \Delta t$ becomes

$$dm(t + \Delta t) = dm(t) + dm_{acc},$$

where dm_{acc} is the amount of accreted matter deposited in the shell of mass $dm(t)$, as coming out from our accretion model.

2.2. Initial models and accretion rates

We have computed the PMS evolution of stars with initial mass M_{ini} of 0.1, 0.2, 0.3, 0.4, 0.5, 0.6, 0.7, 0.8, 0.9, 1.0, 1.1, 1.2, 1.3, 1.4, 1.5, 1.7, 2.0, and $2.5 M_{\odot}$, with metallicity $Z = 0.02$ and He mass fraction Y equal to 0.293 (scaled from Anders & Grevesse 1989). Our initial models result from a polytropic model with polytropic index $n=1.5$ and after convergence with our stellar evolution code, the central temperature T_c is of a few 10^5 K in all cases. Accretion parameters are $Ri^- = -10^4$, $\mathcal{E}^a = 0.75$, $\alpha = 0.1$ and $\xi = 0.01$ (see Paper I for their meaning). They contribute to uniformly distribute the material inside the convective envelope. The value $\alpha = 0.1$ is chosen in such a way that most of the accretion energy released in the boundary layer is radiated away.

If we consider a typical effective accretion rate $\dot{M}_{acc} \simeq 10^{-7} M_{\odot} \text{ yr}^{-1}$ and a process lasting $\sim 5 \cdot 10^6$ yr, about $0.5 M_{\odot}$ is accreted by the star. Adopting this value as the average mass of circumstellar matter surrounding PMS stars, we investigate the structural response of the star to (i) a constant accretion rate $\dot{M}_{acc} = 10^{-7} M_{\odot} \text{ yr}^{-1}$ during $4.5 \cdot 10^6$ years followed by an exponential decrease with characteristic time scale $\tau = 5 \cdot 10^5$ yr (case A) and to (ii) an exponentially decreasing accretion rate given by $\dot{M}_{acc} = 10^{-6} \exp(-t/2.10^5) + 10^{-7} \exp(-t/3.10^6)$ (case B). This last expression accounts for a large accretion phase at the beginning of the evolution followed by a slowly decreasing accretion activity.

This study is devoted to low-accretion rates but we must mention that some T Tauri stars are subject to periodic, short-timed and high accretion rates, so called Fu Ori outburst (see e.g. Hartmann & Kenyon 1996). Notably, Hartmann et al. (1997) suggest that these powerful events are responsible for the main mass accretion during the PMS life. This represents another case that will be analyze in a forthcoming paper dedicated to high accretion rates. Finally, let us point out that the accretion geometry does not resume to boundary layers, as we assume

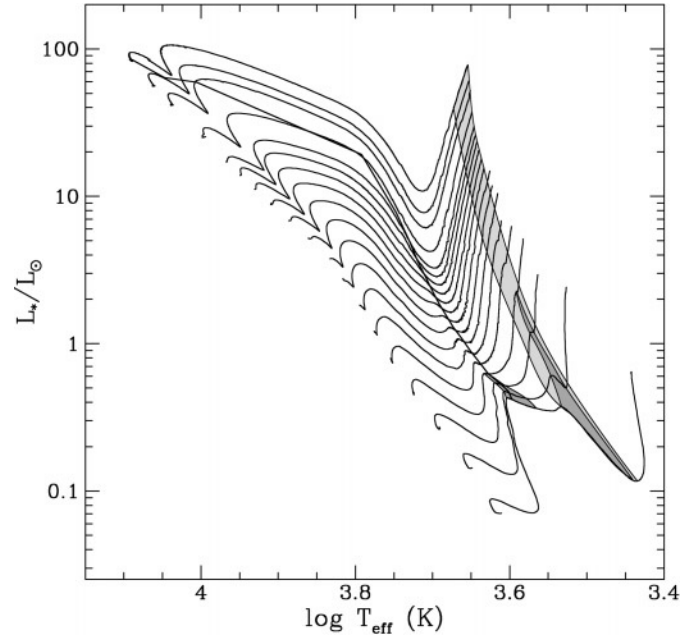


Fig. 1. The HRD evolutionary tracks of $Z = 0.02$ accreting stars of initial masses (from the right to the left) $M_{ini} = 0.1, 0.2, 0.3, 0.4, 0.5, 0.6, 0.7, 0.8, 0.9, 1.0, 1.1, 1.2, 1.3, 1.4, 1.5, 1.7, 2.0,$ and $2.5 M_{\odot}$. The accretion rate is constant and equal to $10^{-7} M_{\odot} \text{ yr}^{-1}$ (case A). The light hatched band at the top of the diagram represents the locus of initial stellar deuterium burning. The dark dashed areas correspond to regions where the gravitational luminosity L_{grav} is negative. At the end of the calculations, each star has accreted $0.5 M_{\odot}$ and has reached its main sequence. The heavy line represents the isochrone corresponding to star age of $4.5 \cdot 10^6$ yr, i.e. at the beginning of the exponential decrease of the accretion rate

here. In the presence of magnetic field, matter can flow in the star along funnel flows or accretion column (e.g. Shu et al. 1994ab, Ferreira & Pelletier 1995).

3. Structure and evolution of accreting PMS stars

HRDs are shown in Figs. 1 and 2 for accretion rates prescriptions A and B, respectively. For comparison, we present in Fig. 3 standard grids of PMS tracks that we will refer to as “standard models” in the following. They were computed with the same metallicity and constitutive physics (Siess et al. 1997b) but without accretion.

Initially, the star supplies its energy loss by a quasi-static contraction until the central temperature T_c reaches $\sim 10^6$ K, which is enough to ignite deuterium burning. The energy released by this transformation is important and the contraction is considerably slowed down. At that stage, the star is fully convective and in a standard scheme the initial deuterium content is completely converted into ^3He in a few 10^4 yr to a few 10^5 yr (depending on the initial mass, M_{ini}).

The arrival of fresh (deuterium rich) material from the accretion disk maintains the nuclear energy production. In the limit where all accreted atoms of deuterium are burned, the generated luminosity is given by

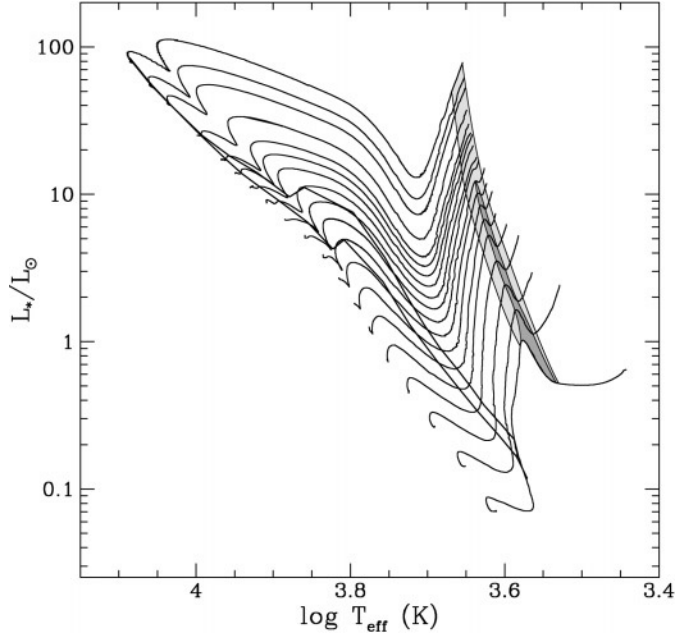


Fig. 2. Same as Fig. 1 but for the bi-exponential accretion law (case B). From upwards, the plotted isochrones correspond to star ages of 10^7 and $1.5 \cdot 10^7$ yr, respectively

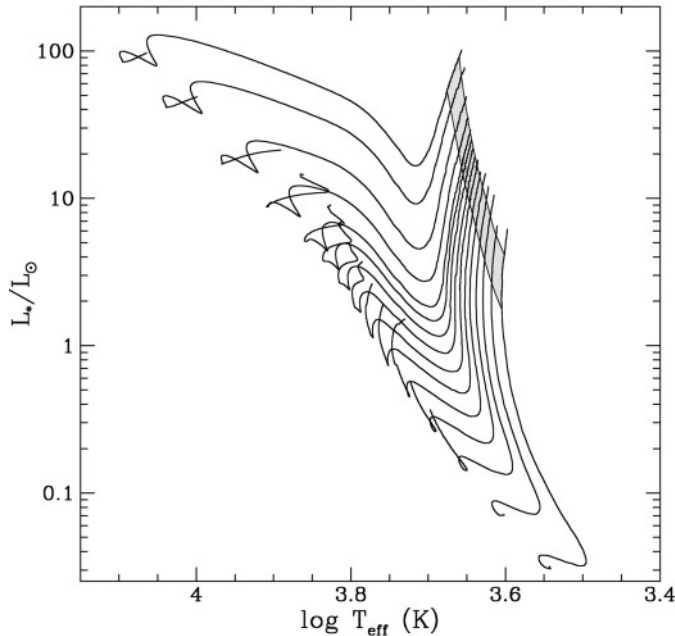


Fig. 3. The evolutionary tracks in the HRD of $Z = 0.02$ “standard” stars of (from the right to the left) 0.5, 0.6, 0.7, 0.8, 0.9, 1.0, 1.1, 1.2, 1.3, 1.4, 1.5, 1.7, 2.0, 2.5 and $3 M_{\odot}$. These models come from Siess et al. (1997b) and will refer to as standard models. Hatched area represents the region of deuterium burning

$$L_D = \mathcal{N}_{av} Y_D^{acc} Q_D \dot{M}_{acc} \simeq 0.2 \frac{\dot{M}_{acc}}{10^{-7}} L_{\odot}, \quad (4)$$

where \mathcal{N}_{av} is the Avogadro number, Y_D^{acc} the deuterium number abundance per mole and per unit mass in the accreted matter and Q_D the energy per unit mass generated per ${}^2\text{H}(p, \gamma){}^3\text{He}$

reaction¹. The rise of the nuclear luminosity is supported by the accretion process and for low-mass stars, the energy released produces a global swelling of the star. Following our computations, expansion occurs for $M_{ini} < 0.4 M_{\odot}$ in case A and $M_{ini} < 0.9 M_{\odot}$ in case B. When the initial content of deuterium is depleted, accretion alone provides the star with deuterium. The nuclear luminosity then reaches its equilibrium value given by Eq. (4) and the star returns to a quasi-static contraction. With the increasing central temperature, the opacity drops and a radiative core develops. During this phase, the burning of light nuclides in the central region (successively ${}^6\text{Li}$, ${}^7\text{Li}$, ${}^9\text{Be}$, ${}^{11}\text{B}$ and ${}^{10}\text{B}$) do not produce energy enough to play an important role. Finally, when the central temperature approaches $1.5 \cdot 10^7$ K, the depletion of ${}^3\text{He}$ and ${}^{12}\text{C}$ starts. The important nuclear energy then released is converted into work against gravity and the contraction is halted.

When the hydrogen burning cycles reach equilibrium, the star enters its main sequence. It is worth noting that in case B the accretion process is maintained during $\sim 1.5 \cdot 10^7$ yr (until $\dot{M}_{acc} < 10^{-9} M_{\odot} \text{ yr}^{-1}$).

4. Comparisons with standard evolution

Comparisons with standard evolution computations can either be made by selecting various quantities at a precise time or from the location of the star in the HRD. All the comparisons made in this section will be done with respect of the Siess et al. (1997b) standard grid of models. The constitutive physics is the same in all the presented computations, observed differences are thus the result of the accretion process alone. In the next section, we first describe the evolution of several variables at a given time.

4.1. Comparing the structure

Stellar evolution with accretion is mainly modified by the combination of two effects, namely (i) the mass addition which contributes to reinforcing the gravitational potential and (ii) the nuclear energy production provided by deuterium burning, which in turn tends to slow down the contraction.

Prior to deuterium ignition ($t < 10^5$ yr), the addition of accreted matter accelerates the contraction of the star. Consequently the central temperature and density increase substantially. However, when deuterium burning ignites, the structural evolution is now much more sensitive to the parameters of our model, especially to the accretion energy deposition (α). For this reason, we divided our study into two parts. On one hand we will deal with low-mass stars ($M_{ini} \lesssim 1.3 M_{\odot}$) where the accretion luminosity can represent a significant fraction of the stellar luminosity and on the other hand with more massive stars ($M_{ini} \gtrsim 1.3 M_{\odot}$) for which the contribution αL_{bl} is negligible with respect to their photospheric luminosity.

¹ The nuclear reaction ${}^2\text{H}({}^2\text{H}, n){}^3\text{He}$ can be neglected because its nuclear flux is much lower than the one associated with the ${}^2\text{H}(p, \gamma){}^3\text{He}$ reaction

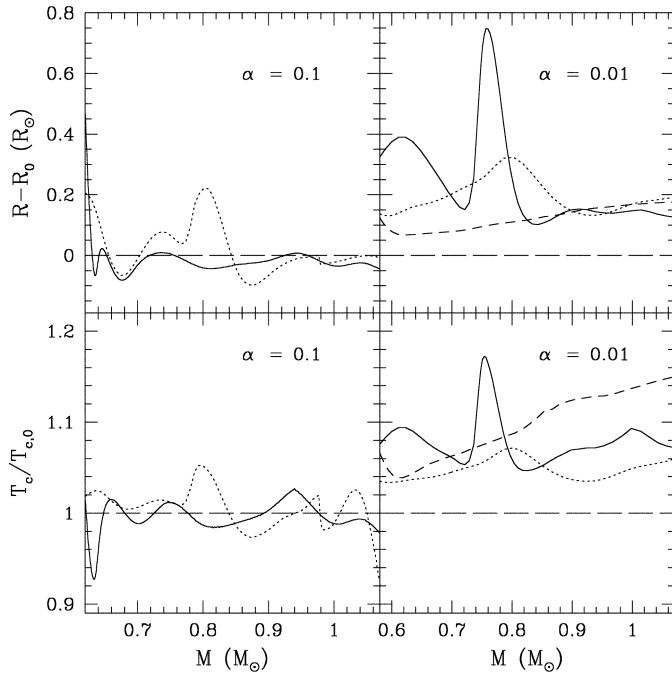


Fig. 4. Comparison of central temperature and radius between low-mass stars with and without accretion. R_0 and $T_{c,0}$ represent the radius and central temperature coming from standard models without accretion (Siess et al. 1997b). The *left panels* correspond to the models provided by our grids with $\alpha = 0.1$, the solid and dotted lines corresponding to cases A and B, respectively. In the *right panels*, the solid, dotted and dashed curves refer to accretion rates equal to $5 \cdot 10^{-6} \exp(-t/4 \cdot 10^5) + 2 \cdot 10^{-7} \exp(-t/2.5 \cdot 10^6)$, 10^{-6} and $10^{-7} M_{\odot} \text{ yr}^{-1}$ and with $\alpha = 0.01$, as defined in Paper II

4.1.1. Low-mass stars

Fig. 4 (right panel) shows that with few accretion energy deposition ($\alpha = 0.01$), an accreting star systematically presents a smaller radius than in a standard evolution. The difference in radii is more pronounced when the accretion rate is higher because in these situations the mechanical effect of mass deposition is reinforced. This shift is also present during the star expansion which results from the nuclear burning of the initial deuterium content. Accreting stars thus present a higher central temperature than standard evolution models, as $T_c \propto M/R$. However these discrepancies reduce as α becomes larger. The accretion energy is then converted principally into work against the compression and consequently the contraction is slowed down and the swelling more important during the main deuterium nuclear burning phase. In such a case, the radius of an accreting star is close to its standard value.

The part of the HRD where the gravitational luminosity becomes negative is indicated by dark hatched areas in Figs. 1 and 2. It concerns stars with initial mass less than $\sim 0.4 M_{\odot}$ and $\sim 0.9 M_{\odot}$ in cases A and B, respectively. This phase of global expansion is longer for the lower mass stars because (i) their lower central temperature leads to a slower deuterium burning and (ii) the accretion luminosity (αL_{bl}) is large and

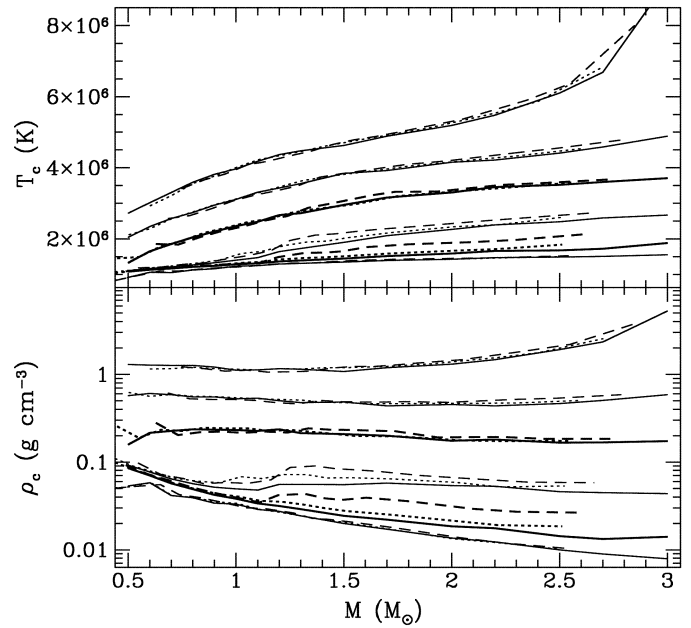


Fig. 5. Central density and temperature as a function of the mass in case of (a) standard evolution (solid line, Siess et al. 1997b), (b) evolution with accretion rates given by A (dotted line) and (c) given by B (dashed line). The selected times, in order of increasing central density or temperature, are $2 \cdot 10^4$, 10^5 , $2 \cdot 10^5$, $5 \cdot 10^5$, 10^6 and $2 \cdot 10^6$ yr, respectively

contributes to increase the negative value of L_{grav} ($L_{grav} = L - L_{nuc} - \alpha L_{bl}$).

With the exhaustion of initial stellar deuterium, the star returns to global contraction, the nuclear luminosity reaches its equilibrium value L_D and the luminosity decreases as long as the star lies on the Hayashi line. Eventually L becomes once more equal to $L_{nuc} + \alpha L_{bl}$. The low-mass star then experiences a new dilatation (at least of the central part of the star) as indicated by the second dashed area in Fig. 1. Finally, with the termination of the accretion process, the star relaxes on the standard PMS track corresponding to its final mass.

4.1.2. Intermediate-mass stars

In more massive stars ($M_{ini} \gtrsim 1.3 M_{\odot}$), the nuclear luminosity due to deuterium burning (L_{nuc}) and the luminosity injected into the star (αL_{bl}) are very small compared to the emergent stellar luminosity and are not sufficient to produce a swelling. The mechanical influence of accretion cannot be balanced by the nuclear energy production or by the deposition of accretion energy.

From Fig. 5, we see that higher accretion rates lead to higher central temperature and density (dashed line). The reason is that young stars are not highly condensed objects and the faster mass accumulates in the star, the more efficient the contraction is. This effect is more important for massive stars that already have a rapid contraction rate.

With increasing initial mass, central temperature is higher so that deuterium ignites earlier and burns more rapidly. For

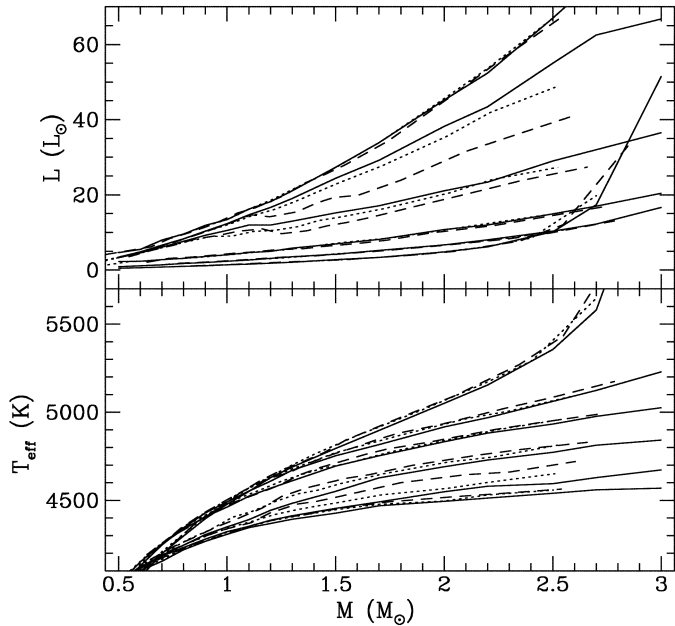


Fig. 6. Same as Fig. 5 but for the effective temperature and stellar luminosity. The selected times in order of increasing T_{eff} or decreasing luminosity are $2 \cdot 10^4$, 10^5 , $2 \cdot 10^5$, $5 \cdot 10^5$, 10^6 and $2 \cdot 10^6$ yr, respectively

example, the deuterium burning phase of a $M_{\text{ini}} = 2 M_{\odot}$ star lasts $\sim 1.5 \cdot 10^5$ yr and $\sim 10^5$ yr in case A and B, respectively. For comparison, a $M_{\text{ini}} = 0.1 M_{\odot}$ star will burn its initial deuterium during $\sim 10^6$ yr and $\sim 5 \cdot 10^5$ yr for the same respective cases A and B.

4.2. Comparisons from the location in the HRD

In the HRD, the motion of a completely convective accreting star is made up of two displacements: (i) the usual vertical shift along the Hayashi line and (ii) an horizontal shift due to the increasing mass. As we have seen above, using the central temperature as an indicator of the evolutionary status of the star, an accreting star evolves more rapidly than in a standard scheme, since its central temperature is higher. Therefore, the star moves downward faster along the Hayashi line and thus exhibits a lower luminosity at a given age than it would in an accretion-less evolution. On the other hand, the enhancement of the stellar mass results in an horizontal displacement and contributes to increase the effective temperature as we can see from Fig. 6. Consequently, the path followed by the star in the HRD is more inclined than in a standard evolution.

Concerning the depth of the convective envelope, we know from Paper II that the development of the radiative core can be delayed by accretion because the radiative gradient ∇_{rad} remains higher than the adiabatic gradient due to the additional nuclear energy production ($\nabla_{\text{rad}} \propto L_r$). But, on the other hand, matter accretion forces the star to evolve more rapidly, so that a radiative core develops more rapidly as well. As a result, we see from Fig. 7 that accretion is not able to maintain a convective envelope that is significantly deeper than in standard evolution.

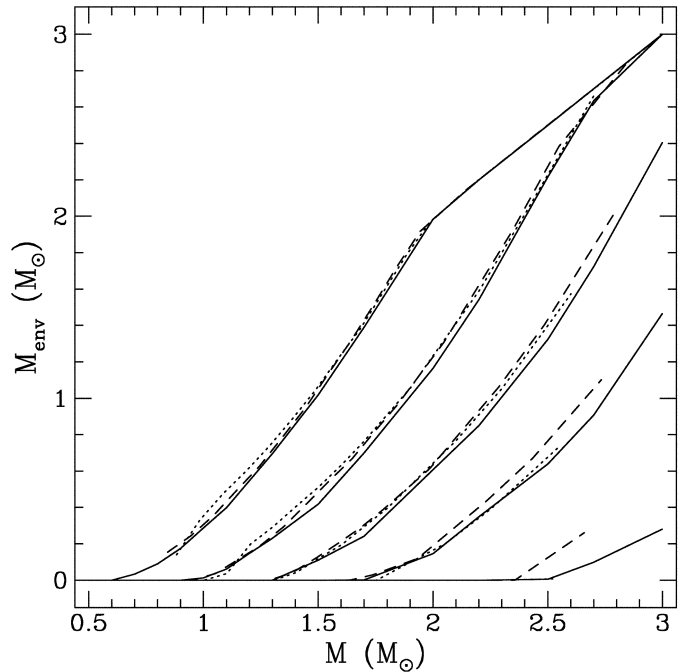


Fig. 7. Mass coordinate of the base of the convective envelope as a function of the total stellar mass. Conventions are the same as in Fig. 5. From the right to the left, the mass of the convective envelope is presented at times $2 \cdot 10^5$, $5 \cdot 10^5$, 10^6 , $2 \cdot 10^6$ and $5 \cdot 10^6$ yr, respectively

Therefore, for the assumed accretion rate and α , accretion does not solve the puzzling problem of strong surface activity encountered in intermediate-mass stars. The activity of Herbig Ae/Be stars is such that they are sometimes assumed to have chromospheres. In low-mass stars, chromospheric activity is linked to the presence of convection in the subphotospheric layers (e.g. Catala 1989) but the nature of activity in intermediate-mass stars remains unknown. Palla and Stahler (1993) found that Herbig Ae/Be stars do follow a convective track for a short time and conclude that the presence of emission lines and strong winds in Herbig Ae/Be stars may not be linked to the outer convective zone, as their models always show that convection retreats towards the surface with increasing effective temperature.

Given position in the HRD, we now compare the mass and age estimates from the standard and variable mass tracks passing through this point, looking for general trends.

- We note that during the convective phase, the age of an accreting star is systematically lower than in a conventional evolution. The discrepancy between these two evolutionary schemes is of order of 10^5 yr and is maximum at the time of stellar deuterium burning (the dark hatched regions in Figs. 1 and 2). During this period, the ages of accreting and non-accreting convective stars differ by a factor 2–3. When the star develops a radiative core, the age determination is made difficult because in this portion of the HRD isochrones are almost parallel to the evolutionary tracks.
- Mass estimate is very similar in both evolutionary schemes, especially when the star is completely convective. However, when entering its radiative track, we observe that mass

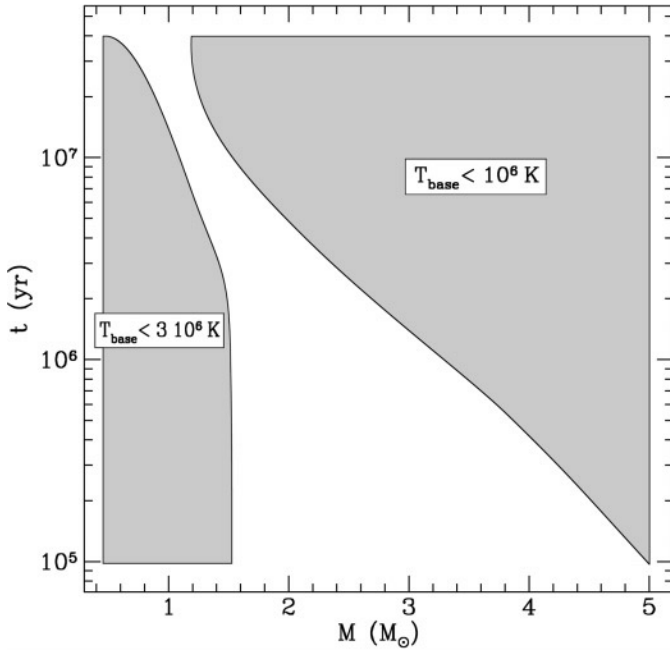


Fig. 8. Time at which the temperature at the base of the convective zone reaches $3 \cdot 10^6$ (left curve) and 10^6 K (right curve) as a function of the mass of the star. These temperatures correspond to the threshold above which ${}^7\text{Li}$ and ${}^2\text{H}$ are nuclearly depleted with convective mixing. The dashed regions represent the locus where accretion can increase the abundances of these elements (see text)

determined from accreting tracks is systematically smaller than the value derived from standard evolution tracks by a few percent ($\Delta M/M \lesssim 5\%$). The discrepancy is more pronounced if the accretion process is maintained for a longer period than in case B.

We now show that accreting tracks can be distinguished from standard evolution by differences in the surface chemical abundances.

5. Effect of accretion on surface chemical abundances

Some light species can be partially or completely depleted at the surface of PMS stars due to their low burning temperatures. ${}^2\text{H}$ and ${}^7\text{Li}$ are expected to be mostly depleted in that respect and accretion can significantly modify their surface abundance depletion. Two situations have to be considered. Either the base of the convective envelope is hot enough to allow nuclear reactions to occur or it is not. For a given element that has been partially or completely depleted during the fully convective phase, accretion will increase its surface abundance to its initial (interstellar) level if no nuclear burning is present inside the convective envelope. The region where the nuclear activity has stopped in the convective envelope (i.e. for temperatures at the base of the convective envelope lower than $\sim 10^6$ K and $3 \cdot 10^6$ K for ${}^2\text{H}$ and ${}^7\text{Li}$, respectively) is represented in Fig. 8 by the hatched area. If accretion occurs when the star evolves in the dark (light) region, ${}^2\text{H}$ (${}^7\text{Li}$) is not destroyed. On the other hand, if the convective envelope is still burning an element when accretion keeps on,

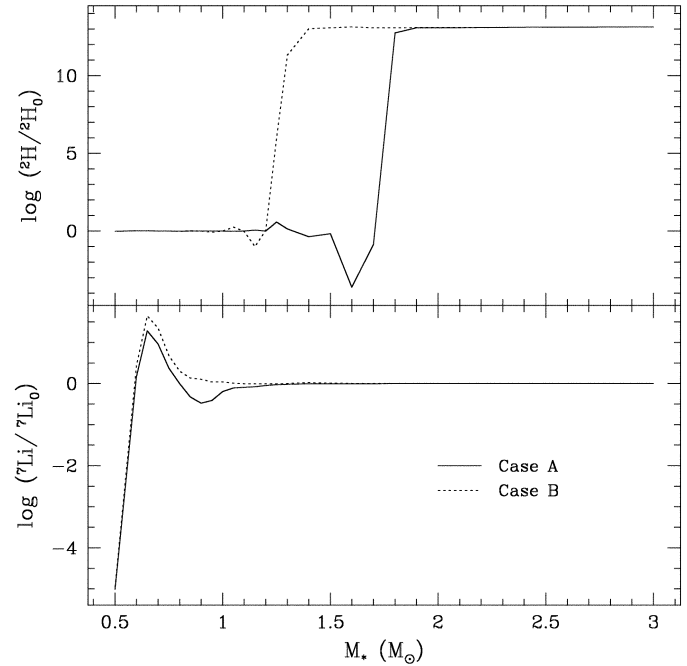


Fig. 9. Surface abundance of ${}^2\text{H}$ and ${}^7\text{Li}$ relative to their standard non accreting values (${}^2\text{H}_0$ and ${}^7\text{Li}_0$, respectively) as the stars reach their ZAMS. The solid and dotted lines refer to the accretion calculations in cases A and B, respectively. Note that on the ZAMS, the ${}^2\text{H}$ abundance in standard models (Siess et al. 1997b) is similar for all masses, the mass fraction being equal to $X({}^2\text{H}_0) \simeq 10^{-18}$

the further evolution of its surface abundance will mainly depends on the ratio between the accretion and nuclear burning time scales (τ_{acc} and τ_{nuc} , respectively). If accretion proceeds at a high rate compared to the nuclear burning rate associated with a specific nuclide ($\tau_{acc} < \tau_{nuc}$), it stops its surface depletion and can even reverse it. On the opposite, if $\tau_{acc} > \tau_{nuc}$, accretion cannot prevent the surface abundance decrease; at most, it slows it down.

5.1. The ${}^2\text{H}$ surface abundance

Fig. 8 tells us that for stars less massive than $\sim 1.2 M_\odot$, deuterium cannot survive in the surface layers as the temperature at the base of the convective envelope always remains higher than 10^6 K. In case A (B), accretion is stopped at times $t \sim 6 \cdot 10^6$ yr ($1.5 \cdot 10^7$ yr) and from Fig. 8, we read that it affects the ${}^2\text{H}$ abundances of stars with $M \gtrsim 1.8 M_\odot$ ($M \gtrsim 1.3 M_\odot$). These results are confirmed in the upper panel of Fig. 9, which depicts the ${}^2\text{H}$ mass fraction as the star reaches the ZAMS. The signature of accretion is clearly obvious and causes the surface ${}^2\text{H}$ abundance to increase almost to its initial interstellar level.

5.2. The ${}^7\text{Li}$ surface abundance

From Fig. 8, we can see that ${}^7\text{Li}$ is never burned in the envelope of stars more massive than $\sim 1.5 M_\odot$. We also note that in the mass range $0.8\text{--}1.0 M_\odot$, accretion in case A (solid line in Fig. 9)

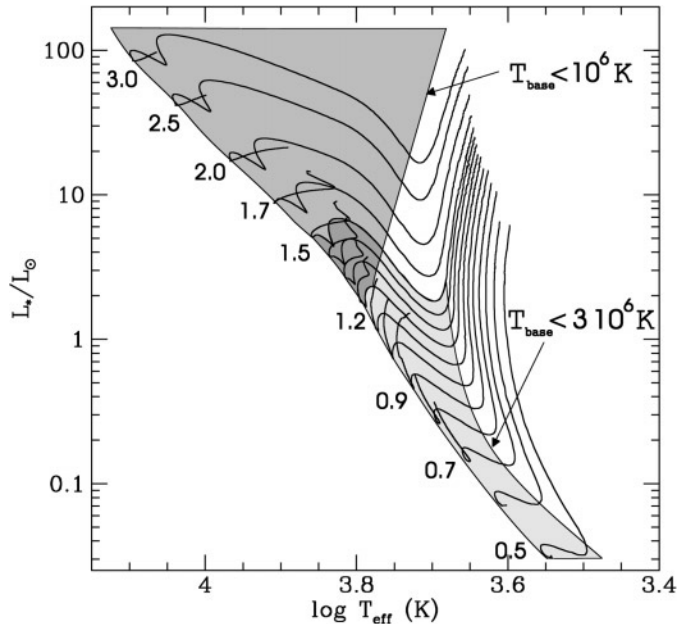


Fig. 10. HR diagram showing the regions where accretion modifies the surface abundances of ${}^7\text{Li}$ and ${}^2\text{H}$. The light area delimited by $T_{\text{env}} < 3 \cdot 10^6$ corresponds to the locus where ${}^7\text{Li}$ surface abundance is increased if accretion is taking place there. Similarly, in the region where $T_{\text{env}} < 10^6$ (dark area), deuterium detection would clearly establish the presence of accretion

favors lithium depletion. Indeed, with higher accretion rates the central temperature reaches larger values and ${}^7\text{Li}$ is burned more efficiently during the fully convective phase. We report a difference of ~ 0.6 dex with respect to the standard value when the stars reach their ZAMS. For lower mass stars ($M \lesssim 0.8 M_{\odot}$), accretion is still taking place when the temperature at the base of the convective envelope falls below $3 \cdot 10^6$ K, resulting in an increase of ${}^7\text{Li}$ surface abundance.

To illustrate these conclusions, we present in Fig. 10 the regions in the HRD where accretion modifies the surface abundances of deuterium and lithium. From the above considerations, we can expect to detect deuterium in young PMS stars with $M \gtrsim 1.2 M_{\odot}$ (dark area) and to observe enhanced lithium surface abundance in young low-mass stars with $M \lesssim 1.5 M_{\odot}$ (light area).

6. Comparison with observations

For the purpose of illustrating our results, we selected a sample of young stars and determined their mass and age, by interpolating the luminosity and effective temperature in the different grids of models. These characteristics have been evaluated from standard evolution models and for the two accretion rates used in the present study. As can be seen from the Table 1, there are several non-determinations denoted by (ind.) which correspond to very low-mass stars ($M \lesssim 0.1\text{--}0.2 M_{\odot}$) located outside our evolutionary tracks. We also note that for stars on their

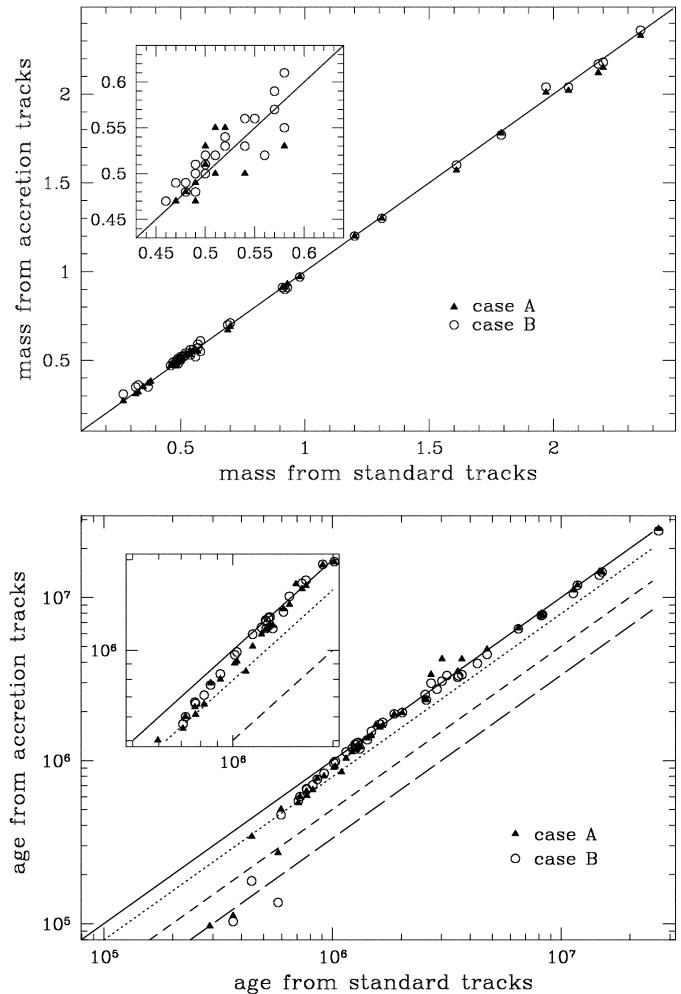


Fig. 11. Mass and age determinations from the different grids of models. Data are compared to the 1:1 relation (solid line) expected from standard tracks. For the age determinations we have also depicted the $t_{\text{acc}} : t_{\text{stand}}$ relations corresponding to 1:1.25 (dotted line), 1:2 (short-dashed line) and 1:3 (long-dashed line)

radiative branch, age determination is relatively uncertain since isochrones are almost parallel to the evolutionary tracks.

6.1. The effect of accretion on age and mass determination

From Fig. 11 (lower panel), we see that for ages $t \lesssim 1.5 \cdot 10^6$ yr accreting stars are effectively younger than standard ones. The deviation from the 1:1 relation is more pronounced for the youngest stars with an age difference varying by a factor 2 or 3. This shift between the difference estimates decreases with time and for $t \gtrsim 1.5 \cdot 10^6$ yr, the dispersion in ages is small, less than $\sim \pm 10\%$, with a linear correlation coefficient > 0.97 .

The stellar mass determination is almost not affected by the presence of accretion. The deviation from the 1:1 relation is very small, the linear correlation coefficient being always larger than 0.999 in both cases A and B. This result is not surprising as the

Table 1. Properties of T Tauri Stars. The Herbig & Bell Catalog numbers (HBC) comes from Herbig & Bell (1988). The effective temperatures are given by Cohen & Kuhn (1979) or determined from the spectral type using the Cohen & Kuhn (1979) conversion relation. The intrinsic luminosity has been estimated by Bouvier (1990), Cabrit et al. (1990) and Bertout (1997). Standard tracks come from Siess et al. 1997b.

Star	Observational points			Standard tracks		Case A		Case B	
	HBC	T_{eff} (K)	L (L_{\odot})	Mass (M_{\odot})	Age (in 10^6 yr)	Mass (M_{\odot})	Age (in 10^6 yr)	Mass (M_{\odot})	Age (in 10^6 yr)
FM Tau	23	3920	0.20	0.66 ± 0.05	12.20 ± 4.11	< 0.72	< 16.60	< 0.72	< 16.10
BP Tau	32	4000	0.96	0.52 ± 0.07	1.02 ± 0.15	0.52 ± 0.07	0.95 ± 0.24	0.52 ± 0.09	0.99 ± 0.23
DE Tau	33	3680	0.43	0.38 ± 0.05	1.55 ± 0.19	0.44 ± 0.07	1.79 ± 0.46	ind.	ind.
RY Tau	34	5780	6.51	1.79 ± 0.08	6.51 ± 0.88	1.78 ± 0.07	6.46 ± 0.81	1.78 ± 0.08	6.37 ± 0.90
T Tau	35	5099	8.81	2.31 ± 0.05	1.32 ± 0.32	2.35 ± 0.08	1.25 ± 0.31	2.35 ± 0.07	1.20 ± 0.31
DF Tau	36	3800	1.84	0.38 ± 0.05	0.29 ± 0.21	0.37 ± 0.06	0.20 ± 0.16	0.42 ± 0.06	0.18 ± 0.14
DG Tau	37	3959	1.35	0.47 ± 0.07	0.71 ± 0.03	0.47 ± 0.07	0.58 ± 0.12	0.49 ± 0.06	0.58 ± 0.11
DH Tau	38	3919	0.41	0.55 ± 0.08	2.86 ± 0.78	< 0.59	< 5.14	< 0.66	< 4.21
DI Tau	39	3919	0.71	0.49 ± 0.07	1.26 ± 0.21	0.48 ± 0.07	1.21 ± 0.29	0.48 ± 0.09	1.21 ± 0.35
UX Tau A	43	4954	1.24	1.30 ± 0.01	8.29 ± 1.65	1.29 ± 0.01	7.87 ± 1.62	1.30 ± 0.01	7.94 ± 1.64
FX Tau	44	3680	0.63	0.35 ± 0.05	1.10 ± 0.01	0.36 ± 0.03	0.86 ± 0.14	ind.	ind.
DK Tau	45	4000	1.38	0.50 ± 0.07	0.72 ± 0.04	0.50 ± 0.07	0.62 ± 0.14	0.51 ± 0.07	0.61 ± 0.11
HL Tau	49	3959	1.22	0.47 ± 0.07	0.77 ± 0.05	0.44 ± 0.10	0.65 ± 0.14	0.50 ± 0.06	0.66 ± 0.14
GG Tau	54	3959	1.13	0.48 ± 0.07	0.82 ± 0.07	0.48 ± 0.07	0.71 ± 0.16	0.50 ± 0.07	0.72 ± 0.16
GH Tau	55	3499	0.69	0.27 ± 0.03	0.58 ± 0.43	0.27 ± 0.04	0.38 ± 0.25	< 0.33	< 0.13
GI Tau	56	4000	0.83	0.53 ± 0.07	1.22 ± 0.22	0.54 ± 0.08	1.18 ± 0.30	0.53 ± 0.08	1.24 ± 0.32
GK Tau	57	4000	1.06	0.51 ± 0.07	0.91 ± 0.12	0.51 ± 0.07	0.84 ± 0.20	0.50 ± 0.08	0.88 ± 0.20
DL Tau	58	3680	1.03	0.33 ± 0.04	0.44 ± 0.30	0.33 ± 0.04	0.32 ± 0.21	0.35 ± 0.02	0.28 ± 0.19
CI Tau	61	4000	0.66	0.55 ± 0.08	1.66 ± 0.39	0.55 ± 0.08	1.73 ± 0.46	0.55 ± 0.09	1.75 ± 0.54
AA Tau	63	3959	0.76	0.51 ± 0.07	1.26 ± 0.23	0.51 ± 0.08	1.22 ± 0.30	0.50 ± 0.09	1.24 ± 0.34
DN Tau	65	3919	0.65	0.49 ± 0.07	1.42 ± 0.28	0.50 ± 0.07	1.42 ± 0.38	< 0.58	< 1.88
DO Tau	67	3959	0.42	0.57 ± 0.08	3.02 ± 0.85	0.59 ± 0.12	4.34 ± 1.29	< 0.69	< 4.44
VY Tau	68	3919	0.33	0.59 ± 0.09	4.30 ± 1.32	< 0.71	< 7.26	< 0.70	< 6.22
Haro 6-3	73	4199	0.84	0.71 ± 0.11	2.02 ± 0.58	0.71 ± 0.10	2.04 ± 0.56	0.71 ± 0.10	2.09 ± 0.53
DR Tau	74	4400	1.06	0.92 ± 0.13	2.54 ± 0.76	0.90 ± 0.13	2.47 ± 0.75	0.91 ± 0.13	2.57 ± 0.76
DS Tau	75	4775	0.42	0.91 ± 0.01	26.70 ± 4.73	0.91 ± 0.01	26.70 ± 4.81	0.90 ± 0.01	26.00 ± 4.76
GM Aur	77	3959	0.75	0.51 ± 0.07	1.29 ± 0.24	0.51 ± 0.07	1.25 ± 0.31	0.50 ± 0.10	1.30 ± 0.38
SU Aur	79	5780	11.74	2.19 ± 0.09	3.68 ± 0.59	2.15 ± 0.09	3.97 ± 0.65	2.18 ± 0.09	3.69 ± 0.64
RW Aur	80	5099	4.47	1.94 ± 0.02	2.57 ± 0.58	1.96 ± 0.05	2.43 ± 0.59	1.94 ± 0.09	2.40 ± 0.59
034903+2	351	4400	0.43	0.92 ± 0.02	11.30 ± 2.98	0.93 ± 0.02	11.30 ± 2.78	0.91 ± 0.03	10.80 ± 2.82
V773 Tau	367	4775	5.59	1.61 ± 0.21	0.85 ± 0.25	1.60 ± 0.21	0.81 ± 0.22	1.59 ± 0.20	0.77 ± 0.20
LkCa-3	368	3680	1.24	0.32 ± 0.04	0.36 ± 0.27	0.32 ± 0.04	0.25 ± 0.17	0.31 ± 0.04	0.20 ± 0.13
LkCa-4	370	4000	0.81	0.53 ± 0.07	1.26 ± 0.24	0.54 ± 0.08	1.22 ± 0.31	0.53 ± 0.08	1.26 ± 0.33
041559+1	376	4000	0.48	0.59 ± 0.09	2.70 ± 0.76	0.70 ± 0.05	3.68 ± 1.26	0.61 ± 0.11	2.92 ± 1.01
V819 Tau	378	4000	0.67	0.55 ± 0.08	1.61 ± 0.38	0.55 ± 0.07	1.67 ± 0.44	0.56 ± 0.09	1.72 ± 0.53
LkCa-7	379	4000	0.72	0.54 ± 0.07	1.48 ± 0.32	0.55 ± 0.08	1.49 ± 0.39	0.55 ± 0.09	1.55 ± 0.45
HD 283572	380	5659	10.28	2.21 ± 0.10	3.53 ± 0.61	2.16 ± 0.10	3.74 ± 0.71	2.19 ± 0.10	3.47 ± 0.64
IP Tau	385	3919	0.36	0.57 ± 0.08	3.56 ± 1.05	< 0.65	< 6.01	< 0.68	< 5.31
042835+1	392	4400	0.37	0.91 ± 0.01	14.70 ± 3.59	0.91 ± 0.01	14.70 ± 3.51	0.90 ± 0.01	14.00 ± 3.53
042916+1	397	4000	0.61	0.56 ± 0.08	1.87 ± 0.47	0.55 ± 0.08	2.03 ± 0.58	0.56 ± 0.10	1.98 ± 0.63
V827 Tau	399	3959	0.74	0.51 ± 0.07	1.30 ± 0.24	0.51 ± 0.07	1.26 ± 0.31	0.51 ± 0.10	1.31 ± 0.38
V826 Tau	400	3959	0.75	0.51 ± 0.07	1.28 ± 0.23	0.51 ± 0.07	1.24 ± 0.31	0.50 ± 0.09	1.26 ± 0.35
V830 Tau	405	3959	0.82	0.50 ± 0.07	1.15 ± 0.19	0.51 ± 0.07	1.08 ± 0.27	0.50 ± 0.09	1.10 ± 0.29
HP Tau/G	415	5899	11.24	2.06 ± 0.08	4.75 ± 0.66	2.02 ± 0.06	4.99 ± 0.57	2.04 ± 0.08	4.44 ± 0.34
LkCa-15	419	4400	0.53	0.95 ± 0.06	8.19 ± 2.30	0.95 ± 0.06	8.24 ± 2.01	0.93 ± 0.05	7.87 ± 2.17
IW Tau	420	4000	1.28	0.50 ± 0.07	0.76 ± 0.06	0.50 ± 0.07	0.67 ± 0.15	0.51 ± 0.07	0.68 ± 0.13
LkCa-19	426	5239	1.19	1.19 ± 0.04	15.10 ± 2.57	1.20 ± 0.04	14.60 ± 2.61	1.20 ± 0.04	14.70 ± 2.60
045251+3	427	4000	0.95	0.52 ± 0.07	1.03 ± 0.16	0.52 ± 0.08	0.96 ± 0.24	0.52 ± 0.09	1.02 ± 0.24
V836 Tau	429	3959	0.41	0.58 ± 0.09	3.17 ± 0.91	< 0.70	< 5.88	< 0.72	< 4.64

star is located at each moment on the standard track corresponding to its instantaneous mass.

6.2. The effect of observational uncertainty

In this section we analyze the changes in M and t determinations caused by the introduction of an observational uncertainty $\Delta T_{\text{eff}} \pm 100$ K on the effective temperature. This uncertainty has several origins and can be related to the observation (conversion between spectral type and effective temperature) and also to the presence of spots on the surface of the star. The temperature of these magnetic structures are 1000–2000 K cooler than the surface stellar temperature, but the effect of starspots on the observed effective temperature is not obvious. Indeed, stellar rotation will more or less dilute the effects of starspots which also depends on their size, surface coverage and temperature. The effect could be at least as large as the uncertainty introduced here.

As illustrated in Fig. 12 (lower panel), we can see that independently of the presence or not of accretion, age determination is very uncertain for the youngest stars. We also note that accretion tends to increase the uncertainty on the age estimate, especially in the period $5 \cdot 10^5 \lesssim t \lesssim 3 \cdot 10^6$ yr where most of the determinations from accretion tracks (filled triangles and open circles) have higher values and are located above standard determinations (crosses). During this time interval, the mean value of $\Delta t/t$ is equal to 20, 26 and 36% in the standard evolutionary models, case A and case B models, respectively. Finally, when the accretion process has terminated ($t \gtrsim 5 \cdot 10^6$ yr), the uncertainties in the age determination become very comparable and close to 20–25% in all evolutionary schemes.

Uncertainties related to the mass determination are globally higher for low-mass stars ($M \lesssim 0.8 M_{\odot}$) with $\Delta m/m \sim 5$ –20%, this value falling below 5% when the mass exceeds $0.8 M_{\odot}$. We also observed that the uncertainty is larger when determinations are made from accreting tracks.

7. Discussion

Hartmann et al. (1997, hereafter HCK) have also considered the effect of accretion on stellar evolution. They assume, as we do, that (i) accretion disturbs only a small area of the stellar surface, either through an accretion disk or a funnel flow, (ii) the transfer of energy between the accreting surface and the stellar photosphere has little effect and (iii) they also account for thermal energy addition by introducing the parameter α , similar in its meaning to ours. But their approach differs significantly from our modeling because they consider that the accretion process affects only the surface layers of the star and also because they use a very simplified modeling of the stellar structure.

Although their study is mainly devoted to high accretion rates, typical of the star forming phase ($\dot{M}_{\text{acc}} \gtrsim 2 \cdot 10^{-6} M_{\odot} \text{ yr}^{-1}$), they also treat lower accretion rates and reach conclusions very similar to ours. As a consequence of a slow accretion process ($\dot{M}_{\text{acc}} = 10^{-7} M_{\odot} \text{ yr}^{-1}$), they found that accreting stars descend their Hayashi branch faster than in nonac-

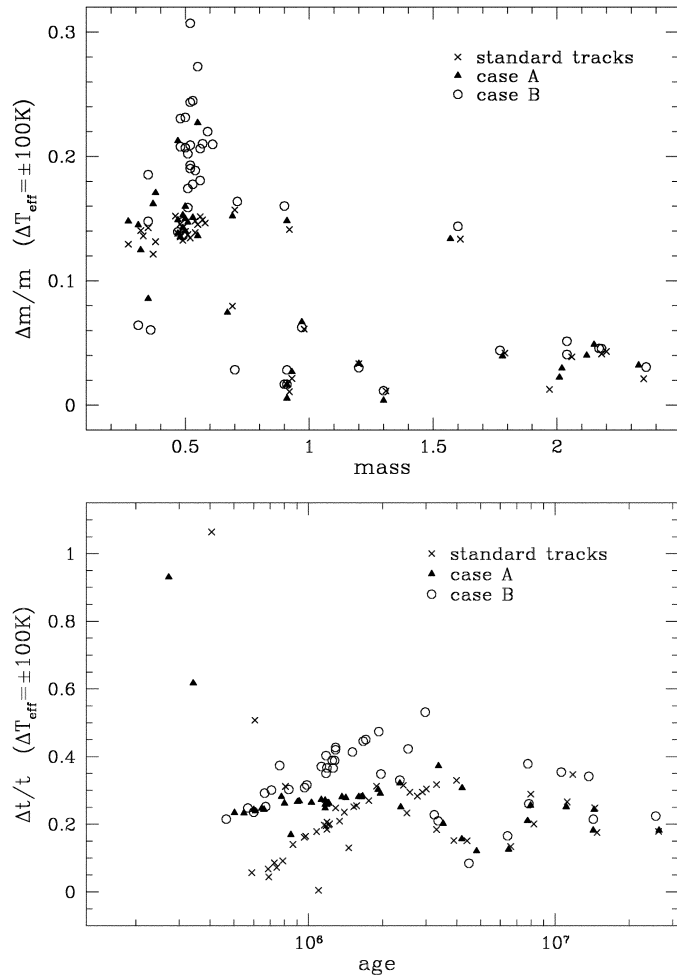


Fig. 12. Errors introduced into the age and mass estimates of our sample due to an observational uncertainty in the effective temperature equal to $\Delta T_{\text{eff}} = \pm 100$ K. The quantity Δm and Δt represents the mean difference in evaluating the mass and time of a star from its position in the HRD shifted by ± 100 K. The values of Δm and Δt are estimated for the standard tracks (crosses) and from accretion tracks A (filled triangle) and B (open circle)

creted evolution, a results confirmed by our study. HCK also noticed (i) large discrepancies between standard and accreting tracks for ages $\lesssim 5 \cdot 10^5$ yr and (ii) that the age of a low-mass star, determined from its location in the HRD, can be overestimated by as much as a factor of 2 for ages $\gtrsim 10^6$ yr. Note however that in their study HCK use a small value of α , which may be more appropriate for funnel flows, because in this scenario, the accreted matter has time to radiate away its thermal excess. They also confirm that thermal energy addition (α larger) leads to an increase of the stellar radius. A straight comparison of their results with ours remains difficult principally because of the different treatment of the stellar structure. However their main results are confirmed by our study, notably the effects of the different parameters and the implications on ages determination of low mass stars.

Another important effect is the geometry of accretion and the physics it involves. In the present paper, we assumed that the

accreted matter joins the star through a boundary layer and, due to shear mixing, can reach the convective zone and be dragged to the center of the star by convective motions. In other accretion geometries, like funnel flows (e.g. Shu et al. 1994ab), the accreted matter is expected to be deposited mainly in the surface layers of the star. In such a case, the fraction α of the accretion energy imparted to the stellar material is deposited in a very thin, low mass region close to the surface. Consequently, if a large amount of energy is released in the stellar atmosphere, one can expect important modifications of the structure of the surface layers and possible recession of the convective zone (Prialnik & Livio 1985), an effect not seen in our computations.

Finally, the study of high accretion rates of the order of $10^{-4}M_{\odot} \text{ yr}^{-1}$, as assumed to prevail in the Fu Ori outburst, is another aspect of accretion onto PMS stars that should be analyzed. During these brief events, a large amount of matter is accreted with probably high values of α ($\gtrsim 0.1$, HCK).

8. Summary

We have presented the evolution of stars accreting a substantial fraction of their mass ($\sim 0.5 M_{\odot}$) during the PMS phase. Chosen accretion timescale and accretion rates have typical values of $5 \cdot 10^6 \text{ yr}$ and $10^{-7} M_{\odot} \text{ yr}^{-1}$, respectively. For the invoked accretion rates, our computations indicate that the contraction rate is globally increased by the mass addition, the star contracts more efficiently and its evolution is accelerated. Consequently the age of a low-mass star, determined from its position in the HRD, can be overestimated by a few 10^5 yr , when using standard tracks without accretion; a conclusion also reached by other groups (Hartmann & Kenyon 1990, HCK, Palla & Stahler 1993). The stellar mass is well determined from the star position in the HRD; the error in its determination does not exceed 5% and does not depend on the evolutionary scheme. Finally, we note that accretion is unable to maintain a deep convective envelope and thus cannot help elucidating the problem of strong stellar activity of intermediate-mass stars.

The clearest signature of accretion is the nucleosynthesis of light elements. The replenishment of fresh material from the accretion disk alters the evolution of the surface chemical abundances of ^2H and ^7Li . Differences in ^7Li surface abundances are expected to be small because its burning occurs late in the evolution. In stars more massive than $1.5 M_{\odot}$, the surface abundance of this element is not modified by the accretion process. For stars around $1 M_{\odot}$, our calculations indicate that ^7Li surface abundance for stars reaching the ZAMS is decreased by ~ 0.6 dex with respect to standard models (Siess et al. 1997b), due to a faster increase of central temperature in their PMS evolution. But the most “visible” and clear signature of accretion is the expected presence of deuterium at the surface of stars more massive than $\sim 1.2 M_{\odot}$. Indeed, in these objects the temperature at the base of the convective zone falls below 10^6 K and prevents deuterium depletion in the surface layers. Therefore, Herbig Ae/Be stars presenting an IR excess, suggesting the presence of an accretion process, are the best candidates for such a detection. In stars less massive than $1.2 M_{\odot}$, how-

ever, deuterium is completely destroyed in the envelope for all investigated mass accretion rates.

Acknowledgements. The authors thank the anonymous referee for constructive comments that clarified and improved the paper. The computations presented in this paper were performed at the “Centre de Calcul Intensif de l’Observatoire de Grenoble” and at “IMAG” on a IBM SP1 computer financed by the MESR, CNRS and Région Rhône-Alpes.

References

- Adams F.C., Emerson J.P., Fuller G.A., 1990, *ApJ* 357, 606
 Anders E., Grevesse N., 1989, *Geochim. Cosmochim. Acta* 53, 197
 Alcalá J.M., Krautter J., Covino E., et al., 1997, *A&A* 319, 184
 Alcalá J.M., Terranegra L., Wichmann R., et al., 1996, *A&AS* 119, 7
 Beckwith S.V.W., Sargent A.I., Chini R.S., Güsten R., 1990, *AJ* 99, 924
 Beckwith S.V.W., Sargent A.I., 1993, In: Levy E.H., Lunine J.I. (eds.) *Protostars and Planets III*. University of Arizona Press, Tucson, p. 521
 Bertout C., 1997, unpublished
 Bertout C., Basri G., 1989, *ApJ* 341, 340
 Bertout C., Harder S., Malbet F., Mennessier C., Regev O., 1996, *AJ* 112, 2159
 Bouvier J., 1990, *AJ* 99, 946
 Bouvier J., Forestini M., Allain S., 1997, *A&A* 326, 1013
 Bouvier J., Rigaut F., Nadeau D., 1997b, *A&A* 323, 139
 Burrows C.J., Stapelfeldt K.R., Watson A.M., et al., 1996, *ApJ* 473, 437
 Cabrit S., Edwards S., Strom S.E., Strom K.M., 1990, *ApJ* 354, 687
 Catala C., 1989, In: *Low Mass Star Formation and PMS Objects*. ESO proceeding, p. 471
 Cameron A.G.W., 1985, In: Black D.C., Matthews M.S. (eds.) *Protostars and Planets II*. Univ. of Arizona Press, Tucson, p. 1073
 Cameron A.G.W., Pine M.R., 1973, *Icarus* 18, 377
 Cohen M., Kuhl L.V., 1979, *ApJS* 41, 743
 DeCampli W.M., Cameron A.G.W., 1979, *Icarus* 38, 367
 Edwards S., Ray T., Mundt R., 1993, In: Levy E.H., Lunine J.I. (eds.) *Protostars and Planets III*. University of Arizona Press, Tucson, p. 567 “Protostars and Planets
 Ferreira J., Pelletier G., *A&A*, 1995 295, 807
 Forestini M., 1994, *A&A* 285, 473
 Galli D., Shu F.H., 1993, *ApJ* 417, 243
 Hartigan P., Edwards S., Ghandour L., 1995, *ApJ* 452, 736
 Hartmann L., Cassen P., Kenyon S.J., 1997, *ApJ* 475, 770, HCK
 Hartmann L., Kenyon S.J., 1990, *ApJ* 349, 190
 Hartmann L., Kenyon S.J., 1996, *ARA&A* 34, 207
 Hayashi C., Nakazawa K., Nakagawa Y., 1985, In: Black D.C., Matthews M.S. (eds.) *Protostars and Planets II*. Univ. of Arizona Press, Tucson, p. 1100
 Herbig G.H., Bell K.R., 1988, *Lick Obs. Bull.* no.1111, 1
 Hillenbrand L.A., Strom S.E., Vrba F.J., Keene J., 1992, *ApJ* 397, 613, HSKV
 Krishnamurthi A., Pinsonneault M.H., Barnes S., Sofia S., 1997, *ApJ* 480, 303
 Lyndell-Bell D., Pringle J.E., 1974, *MNRAS* 168, 603
 Neuhäuser R., Sterzik M.F., Schmitt J.H.M.M., Wichmann R., Krautter J., 1995a, *A&A* 295, L5
 Neuhäuser R., Sterzik M.F., Schmitt J.H.M.M., Wichmann R., Krautter J., 1995b, *A&A* 297, 391
 Palla F., Stahler S.W., 1993, *ApJ* 418, 414

- Prialnik D., Livio M., 1985, MNRAS 216, 37
- Safranov V.S., Ruzmaikina T.V., 1985, In: Black D.C., Matthews M.S. (eds.) Protostars and Planets II. Univ. of Arizona Press, Tucson, p. 959
- Shu F.H., Najita J., Ruden S.P., Lizano S., 1994a, ApJ 429, 797
- Shu F.H., Najita J., Ostriker E., et al., 1994b, ApJ 429, 781
- Siess L., Forestini M., 1996, A&A 308, 472, Paper I
- Siess L., Forestini M., Bertout C., 1997a, A&A 326, 1001, Paper II
- Siess L., Forestini M., Dougados C., 1997b, A&A 324, 556
- Strom K.M., Strom S.E., Edwards S., Cabrit S., Skrutskie M.F., 1989, AJ 97, 1451
- Strom S.E., 1995, Rev.Mex.A&A Conf. Ser., Vol. 1, p. 317
- Strom S.E., Edwards S., 1993, In: Phillips J.A., Thorsett J.E., Kulkarni S.R. (eds.) Planets Around Pulsars. ASP Conference Series, Vol. 36,
- Walter F.M., Brown A., Mathieu R.D., Myers P.C., Vrba F.J., 1988, AJ 96, 297
- Wichmann R., Krautter J., Schmitt J.H.M.M., et al., 1996, A&A 312, 439
- Wichmann R., Krautter J., Covino E., et al., 1997, A&A 320, 185
- Wolk S.J., Walter F.M., 1996, AJ 111, 2066
- Yorke H.W., Bodenheimer P., Laughlin G., 1993, ApJ 411, 274
- Yorke H.W., Bodenheimer P., Laughlin G., 1995, ApJ 443, 199